nature communications

Article

https://doi.org/10.1038/s41467-025-56874-y

Unveiling the role of South Tropical Atlantic in winter Atlantic Niño inducing La Niña

Received: 10 July 2024

Accepted: 5 February 2025

Published online: 13 February 2025

Check for updates

Guangli Zhang[1,5], Jiepeng Chen[2,5], Hanjie Fan[3], Lei Zhang[2,4], Mengyan Chen[2,4], Xin Wang[2,4] ✉ & Dongxiao Wang[1] ✉

The boreal winter-peaked Atlantic Niño/Niña can influence La Niña/El Niño (the cold/warm phase of El Niño-Southern Oscillation, ENSO) in the following year. However, the Atlantic Niño-La Niña relationship is more uncertain than the Atlantic Niña-El Niño counterpart. Here, we show that this uncertainty arises from two distinct types of Atlantic Niño events: the Equatorial and Expanded types, which differ in their meridional sea surface temperature (SST) warming. The Equatorial type, with SST warming confined to the equator, has a weaker climate impact due to limited influence on local convective heating in spring when the intertropical convergence zone (ITCZ) shifts southward. In contrast, the Expanded type, with SST warming extending into the southern tropical Atlantic (STA), drive persistent local anomalous convection heating and strong remote atmospheric responses in the tropical Pacific from winter to spring. Our results emphasize the critical role of STA conditions in shaping the influence of winter Atlantic Niño on the Pacific.

The Atlantic Niño/Niña is the dominant mode of interannual variability in the tropical Atlantic[1–6], similar to the El Niño Southern Oscillation (ENSO) in the Pacific. The Atlantic Niño is characterized by reduced trade winds, deepened thermocline depth, and warm sea surface temperature (SST) anomalies in the central to eastern equatorial Atlantic, also known as Atlantic Niño. Conversely, the negative phase, known as Atlantic Niña, is essentially symmetric to Atlantic Niño[7]. Previous studies have typically assessed the intensity of Atlantic Niño/Niña using ATL3 index (SST anomalies in 20°W–0, 3°S–3°N), similar to the approach for evaluating ENSO. The ATL3 index usually exhibits its highest variability during June-July-August (JJA), influenced by intensified southeast trade winds and the shallowest equatorial thermocline depth of the year. Furthermore, a secondary peak of Atlantic Niño/Niña emerges in December-January-February (DJF) as a result of the seasonal intensification of easterly winds[8]. Some of the DJF-peaked Atlantic Niño/Niña events are independent from JJA-peaked events[9], while some of them are extensions of JJA-peaked events[10].

Both JJA-peaked and DJF-peaked Atlantic Niño/Niña events can exert significant impacts on the surrounding[11–14]. Through the atmospheric bridge, Atlantic Niño/Niña can also influence the climate systems of the Indian Ocean and the Pacific Ocean[10,15–19]. In particular, it is proposed that the Atlantic Niño/Niña enhances the likelihood of opposite-signed ENSO events in the subsequent seasons through a westward route[9,20–24]. During an Atlantic Niño event, there is anomalous convergence in the upper levels over the western tropical Atlantic, which modulates the global Walker Circulation and triggers low-level easterly wind anomalies over the western tropical Pacific. The easterly anomalies can induce equatorial upwelling Kelvin waves and cool the SST over the central-eastern Pacific in the subsequent seasons. Through this process, Atlantic Niño/Niña can enhance the prediction capabilities for ENSO events[22,25–33]. However, there is still an ongoing debate regarding the impacts of Atlantic Niño/Niña on subsequent ENSO. Some studies have suggested that Atlantic Niño induces eastward atmospheric Kelvin waves through the Indian Ocean and Maritime Continent, leading to low-level easterlies over the western Pacific

[1]School of Marine Sciences, Sun-Yat Sen University, Southern Marine Science and Engineering Guangdong Laboratory (Zhuhai), Zhuhai, China. [2]State Key Laboratory of Tropical Oceanography, South China Sea Institute of Oceanology, Chinese Academy of Sciences, Guangzhou, China. [3]School of Atmospheric Sciences, Sun Yat-sen University, Southern Marine Science and Engineering Guangdong Laboratory (Zhuhai), Zhuhai, China. [4]Global Ocean and Climate Research Center, South China Sea Institute of Oceanology, Chinese Academy of Sciences, Guangzhou, China. [5]These authors contributed equally: Guangli Zhang, Jiepeng Chen. ✉e-mail: wangxin@scsio.ac.cn; dxwang@mail.sysu.edu.cn

and subsequent La Niña conditions[21,34]. However, the impacts of Atlantic Niño/Niña on ENSO are found to be weak in some models[22,35], especially during the developing phase of ENSO. Therefore, some studies suggested that the Atlantic Niño/Niña has limited ability to promote ENSO development[35]. Besides, a recent study has argued that the apparent relationship between Atlantic Niño/Niña and subsequent ENSO may be a statistical artifact of ENSO's high autocorrelation, since the Atlantic Niño/Niña might be affected by early-onset ENSO[36]. Further analysis is needed to verify the relationship between Atlantic Niño/Niña and subsequent ENSO events.

In fact, the Atlantic Niño/Niña-ENSO connection has been somewhat uncertain in past decades[9,28,31]. The relationship between the JJA-peaked Atlantic Niño/Niña and subsequent ENSO has been strengthened since the 1970s climate shift[22,31,36–38], which could be attributed to the phase transition of the Atlantic Multidecadal Oscillation[39] or interdecadal changes in the Atlantic–South America–Pacific mean state[28]. In addition to the background climatology modulation, the emergence of a central type of Atlantic Niño, which has a stronger influence on tropical climate than its eastern counterpart, has contributed to maintaining a stable Atlantic Niño/Niña-ENSO relationship in the recent decades[30].

Most previous studies have focused on the JJA-peaked Atlantic Niño/Niña due to its stronger amplitude in that season. However, the DJF-peaked Atlantic Niño/Niña exhibits a more pronounced negative correlation with subsequent ENSO events over the past decades (Fig. 1a) despite its slight lower intensity compared to its JJA-peaked counterpart[23]. Furthermore, climate models show that the influence of DJF-peaked Atlantic Niño/Niña events on subsequent ENSO will persist into the future, in contrast to decreased impacts of JJA-peaked events[40]. In this view, we analyzed the relationship between the DJF-peaked Atlantic Niño/Niña and following ENSO from 1950 to 2022. Although all the Atlantic Niño/Niña events exhibit significant SST anomalies in the ATL3 region, some events have SST anomalies limited to the equator, while others can extend to the south tropical Atlantic (STA). Our findings suggest that the SST anomalies in STA region could potentially act as a stabilizing anchor, effectively mitigating the uncertainties of the Atlantic Niño-La Niña relationship.

Results

Uncertain relationship between winter Atlantic Niño and subsequent La Niña

A lead-correlation analysis spanning from 1950 to 2022 shows that the largest negative correlation coefficient between the ATL3-index and DJF-averaged Niño 3.4 index is observed when the ATL3-index leads ENSO by around 12 months (Fig. 1a). Figure 1b shows the respective connections between the Atlantic Niño/Niña in DJF_0 season with El Niño/La Niña in DJF_1 season (where 0 and 1 denote the peak season of winter Atlantic Niño/Niña and ENSO, −1 refers to the preceding year of DJF-peaked Atlantic Niño/Niña). Interestingly, the scatter plot depicting winter Atlantic Niño/Niña and subsequent ENSO reveals an evident

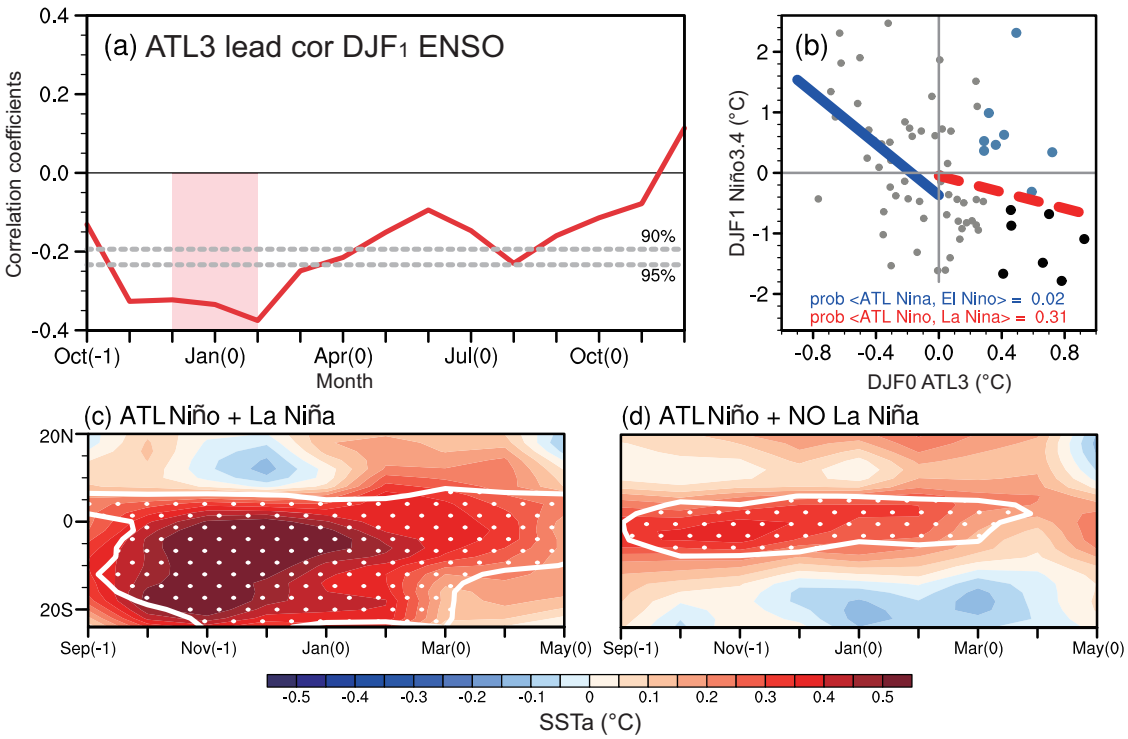

Fig. 1 | Relationship between the Atlantic Niño and subsequent El Niño-Southern Oscillation (ENSO). a Lead coefficient between the ATL3 index (3°S–3°N, 20°W–0°) and Niño 3.4 index (5°S–5°N, 170°W–120°W) in $December_0$-$January_1$-$February_1$ (DJF_1, where −1, 0, and 1 represent the preceding, current and subsequent year of the winter Atlantic Niño peak season) season during 1950–2022. The gray dashed lines indicate thresholds of 90% and 95% confidence levels. **a** Lead coefficient between the ATL3 index (3°S–3°N, 20°W–0°) and Niño 3.4 index (5°S–5°N, 170°W–120°W) in $December_0$-$January_1$-$February_1$ (DJF_1, where −1, 0, and 1 represent the preceding, current and subsequent year of the winter Atlantic Niño peak season) season during 1950–2022. The gray dashed lines indicate thresholds of 90% and 95% confidence levels. The pink shading is DJF_0 season. **b** Scatter plot of Niño 3.4 index in DJF_1 and ATL3 index in DJF_0. The red/blue lines represent regression lines for the scatter based on positive/negative ATL3-indices, with solid/dashed lines indicating fitting coefficients exceeding/not exceeding 95% significance level. The significance level of blue/red lines are 0.02/0.31. Black dots denote years that the ATL3-index in DJF_0 season exceeds its 0.75 standard deviations and Niño 3.4 index in DJF_1 season is lower than −0.5 °C. Blue dots are same as black dots, but for years that Niño 3.4 index in DJF_1 season is higher than −0.5 °C. Composited sea surface temperature (SST, °C, ERSST datasets) anomalies over the tropical Atlantic (40°W–20°E averaged) from $September_{-1}$ to May_0 for **c** Atlantic Niño years followed by La Niña (1950, 1964, 1967, 1973, 1988, 1998 and 2020), **d** Atlantic Niño years not followed by La Niña (1952, 1961, 1963, 1969, 1982, 2004, 2017, 2019). White dots in (**c**, **d**) indicate significance exceed 95% level.

nonlinear behavior. Specifically, most Atlantic Niña events tend to precede El Niño in the following year, whereas Atlantic Niño does not exhibit a clear preference for La Niña conditions in the subsequent winter.

To examine more closely the non-significant relationship between boreal winter Atlantic Niño events and subsequent La Niña occurrences, we divided the DJF-peaked Atlantic Niño events into two groups: those followed by La Niña (black dots in Fig. 1b) and not followed by La Niña (blue dots in Fig. 1b) in the subsequent winter. For Atlantic Niño events followed by La Niña, warm SST anomalies emerge not only in the equatorial Atlantic (EqA) region but also expand to the STA since October$_{-1}$ (Fig. 1c). In contrast, during years when winter Atlantic Niño not followed by La Niña, warm SST anomalies only appear in the EqA region since October$_{-1}$ to early March$_0$, accompanied by weak cold SST anomalies in 10°S–20°S (Fig. 1d).

The different evolutions of SST anomalies in the STA region suggest that anomalous conditions in STA region might be crucial in modulating the relationship between winter Atlantic Niño and subsequent La Niña. In the following, the Atlantic Niño is classified into two types based on the latitudinal expansion of warm SST anomalies: the Equatorial type and the Expanded type ("Methods") to explore their impacts on the tropical Pacific.

Distinct evolutions of the Equatorial and Expanded Atlantic Niño events

By considering the SST anomalies in both the EqA and STA regions, a total of eight Equatorial and eight Expanded Atlantic Niño events from 1950 to 2022 are identified. Among them, 3 out of 8 (38%, Fig. 2a) of Equatorial Atlantic Niño and 7 out of 8 (88%, Fig. 2g) Expanded Atlantic Niño are followed by cold SST anomalies in the Niño 3.4 region in the subsequent winter. The Equatorial and Expanded Atlantic Niño events exhibit distinct evolution processes (Supplementary Fig. 1). The Equatorial Atlantic Niño events are characterized by SST anomalies that remain confined within the tropics from JJA$_{-1}$ to DJF$_0$

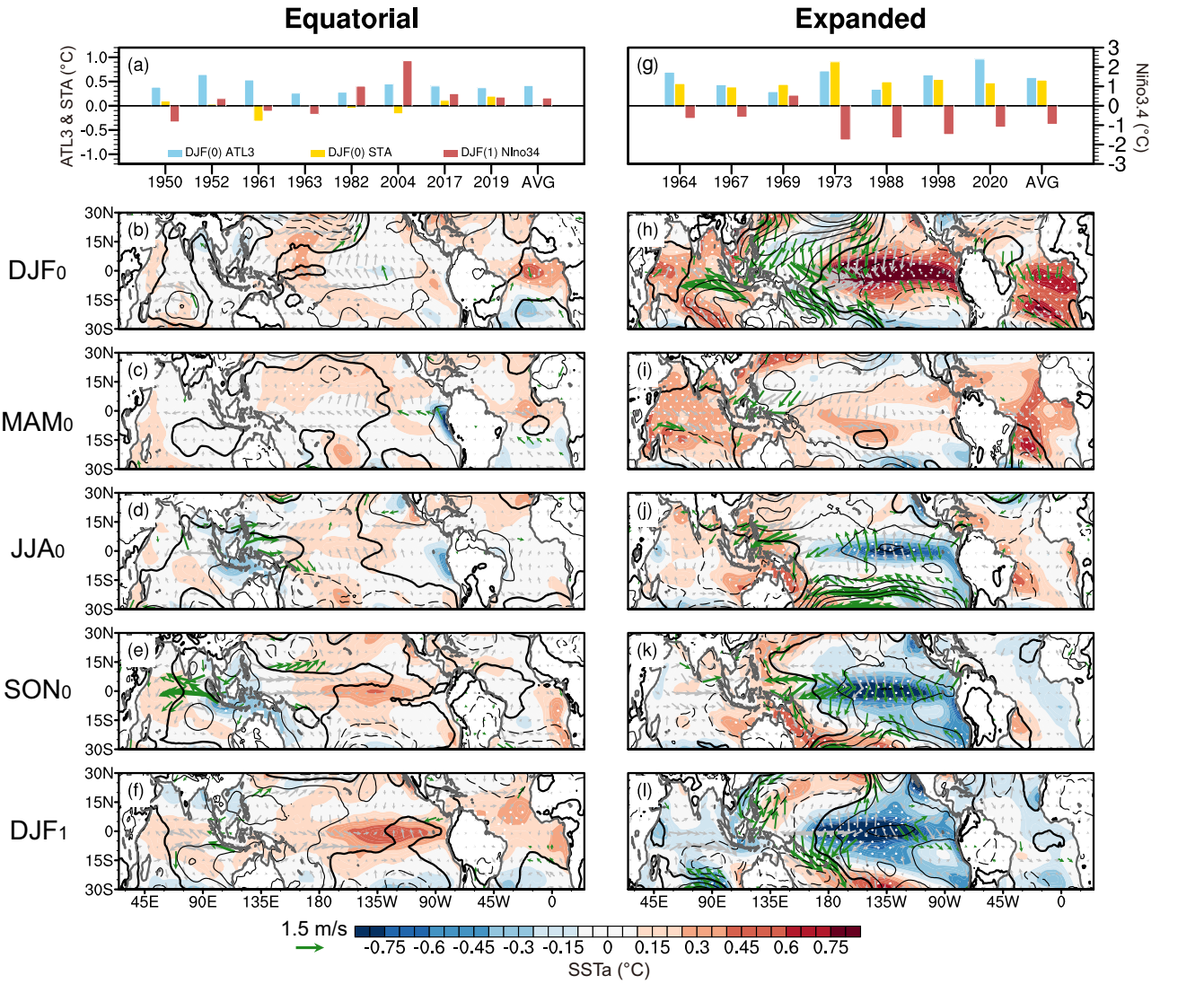

Fig. 2 | Effects of two types of Atlantic Niño events on following El Niño-Southern Oscillation (ENSO). a The Equatorial Atlantic (EqA) index in December$_{-1}$-January$_0$-February$_0$ (DJF$_0$, where −1, 0, and 1 represent the preceding, current and subsequent year of the winter Atlantic Niño peak season) season (blue bar, °C), south tropical Atlantic (STA) index in DJF$_0$ season (golden bar, °C) and Niño 3.4 index in DJF$_1$ season (red bar) for Equatorial type Atlantic Niño events. Years in X-axis indicate the 0 year. **b**–**f** Evolutions of composited sea surface temperature (SST, shading, °C, ERSST), 10 m wind (vectors, m/s, ERA5) and sea level pressure (contour, hPa, thick line indicates the zero contour and interval is 0.3, ERA5) anomalies for Equatorial Atlantic Niño events during DJF$_0$, March$_0$-April$_0$-May$_0$ (MAM$_0$), June$_0$-July$_0$-August (JJA$_0$), September$_0$-October$_0$-November$_0$ (SON$_0$) and DJF$_1$ seasons respectively. The white-dotted regions and black vectors exceed 95% confidence level. **g**–**l** Same as **a**–**f**, but for 7 Expanded Atlantic Niño events.

(Supplementary Fig. 1a–c). Concurrently, surface wind anomalies converge in the western-central equatorial Atlantic, particularly during September-October-November$_{-1}$ (SON), promoting the development of warm SST anomalies in the central-eastern equatorial Atlantic. In contrast, the evolution of the Expanded Atlantic Niño events is more complex from JJA$_{-1}$ to DJF$_0$ (Supplementary Fig. 1d–f). Initially, during JJA$_{-1}$, warm SST anomalies also primarily emerge on the equator, notably in the northern Gulf of Guinea (Supplementary Fig. 1d). By SON$_{-1}$, however, westerly wind anomalies become dominant over the tropical-to-subtropical southern Atlantic, which aids in the expansion of SST warming from the equator to almost 30°S in the subsequent seasons (Supplementary Fig. 1e, f). The intensification of these westerly wind anomalies is linked to an anomalous cyclone in the midlatitudes, potentially a consequence of the weakened climatological South Atlantic anticyclone (SAA)[41].

The SAA is a vast system linking the southern subtropical Atlantic with the equatorial Atlantic regions. A decreasing of the SAA is associated with warming in the east and with cooling in the west, weakening the subtropical zonal SST gradient and maintaining negative SAA strength. The SAA has been hypothesized to facilitate the development of Atlantic Niño/ Niña events following the onset of SST anomalies in the southern subtropical Atlantic[41–44]. However, the SAA strength (as indicated by sea level pressure over 40°S to 20°S and 30°W to 10°W)[43] shows different evolutions during the developing stages of Equatorial/ Expanded Atlantic Niño events (Supplementary Fig. 2). The SAA anomaly is weak during Equatorial Atlantic Niño events since the warm SST anomalies are confined in equatorial region (Supplementary Fig. 2a). In comparison, the SAA has been weakening since August$_{-1}$ and reached its lowest value in November$_{-1}$, leading the peak phase of Expanded Atlantic Niño event by about two months, suggesting the important role of SAA in generation of Expanded Atlantic Niño (Supplementary Fig. 2b).

Additionally, an anomalous SST mode over the Angola Benguela area (ABA: 20°S–10°S, 8°E–15°E, black box in Supplementary Fig. 1)[45], referred to as Benguela Niño/Niña and peaking in the MAM season, is suggested to be a precursor to JJA-peaked Atlantic Niño/Niña events through its coupling with the SAA[42,44,46]. However, prominent warm SST anomalies appear in the ABA region during SON$_{-1}$ season, coinciding with both the DJF-peaked Equatorial and Expanded Atlantic Niño events (Supplementary Fig. 1b, e). With the decline of the anomalous SAA, the warm ABA SST anomalies rapidly dissipate in the DJF$_0$/MAM$_1$ season during Equatorial Atlantic Niño events (Fig. 2b, Supplementary Fig. 1c) and Expanded Atlantic Niño events (Fig. 2i). Considering the shallow thermocline depth along the western African coast (Supplementary Fig. 1g–i), these warm ABA SST anomalies may arise from the extensive surface wind anomalies associated with the weakening of the SAA, which occurs in tandem with the warming of the equatorial Atlantic.

It should be noted that the Expanded Atlantic Niño is accompanied by prominent warming over the central-eastern equatorial Pacific (Fig. 2h). As indicated by previous study, El Niño has thermodynamic warming impact on the tropical Atlantic region, thus an early emerged El Niño might induce an Atlantic Niño[3]. With the fully manifest of the El Niño, the significant Atlantic Niño/Niña-ENSO relationship might be a statistical artifact of ENSO's autocorrelation[47]. In order to check the role of ENSO on Atlantic Niño events, outputs from the CESM2 Pacific Pacemaker experiments conducted by the National Center for Atmospheric Research (NCAR) are further analyzed. In these experiments, the observed ENSO variability is preserved in each simulation, with ENSO acting as the pacemaker, while the rest of climate system is allowed to evolve freely (see "Methods"). Supplementary Fig. 4 shows the composite SST anomalies in the Equatorial and Expanded Atlantic Niño years from the CESM2 Pacific pacemaker experiments. During the Equatorial Atlantic Niño years, warm SST anomalies over the equatorial Atlantic during DJF$_0$ and MAM$_0$ seasons are triggered by cold SST anomalies over the central equatorial Pacific (Supplementary Fig. 4a, b). Conversely, during the Expanded Atlantic Niño years, despite the presence of a strong warm SST anomaly over the central-eastern tropical Pacific, its impact on the equatorial Atlantic and STA regions is found to be minimal (Supplementary Fig. 4c, d). These results indicate that the previous ENSO might induce tropical Atlantic warming in certain years. However, the DJF-peaked Expanded Atlantic Niño events, especially the associated STA warming, are improbable to stem from the impact of ENSO.

Different impacts on subsequent La Niña from the Equatorial and Expanded Atlantic Niño events

Although both the Equatorial and Expanded Atlantic Niño events display peak SST anomalies during DJF$_0$ (Fig. 2b, h), the evolutions of local precipitation responses over the Amazon-western Atlantic region as well as wind and SST responses over the tropical Pacific diverge significantly, especially from May onward (Fig. 3a, d). The Equatorial Atlantic Niño events are marked by more intense precipitation anomalies with a maximum center near the equator during late winter. As the driving SST anomalies begin to weaken since MAM$_0$ (Fig. 2c), the positive rainfall center likewise diminishes and shifts northward, while a weak negative rainfall center develops near 5°S during JJA$_0$ (Fig. 3a). On the other hand, despite the weakening of SST anomalies for the Expanded Atlantic Niño event in MAM$_0$, the SST warming in the STA region remain significant in this season (Fig. 2i). More interestingly, the associated positive precipitation anomalies over the Amazon-western Atlantic region exhibit a double-peaked structure with a noticeable secondary peak during MAM$_0$ (Fig. 3d), which is absent for the Equatorial events.

The different evolutions of precipitation responses can be ascribed to the seasonal meridional shifts of the Atlantic mean state. Notably, the warm SST (higher than 26.5 °C) and intertropical convergence zone (ITCZ) reach their southernmost latitude in MAM and move northward from May (Fig. 3g, Supplementary Fig. 5). Given that the atmospheric responses to the SST anomalies tend to intensify in regions with deep convection[37], the southward shift of the ITCZ could amplify the impact of STA SST anomalies on producing anomalous diabatic heating during the spring season. This interaction between the mean ITCZ and the STA SST anomalies in spring is referred as the "Spring Deep Convection" (SpDC) mechanism in the following sections. Nevertheless, we do not intend to exclude the potential influence of equatorial SST anomalies in triggering atmospheric teleconnections to the Pacific. A detailed examination of the relative contributions of equatorial and STA SST anomalies is presented in the "Discussions" through an analysis of the characteristics of "pure" STA events.

The atmospheric responses of the two types of Atlantic Niño events in the tropical Pacific differ greatly due to their associations with different diabatic heating forcings. For the Equatorial Atlantic Niño events, the weak precipitation response exhibits weak and insignificant convergence locally in the spring season (Fig. 3a), thereby exerting a limited influence on large-scale circulation. As a result, two divergent centers emerge in the eastern tropical Pacific and eastern Indian Ocean, accompanied by a convergence center in the western tropical Pacific (Fig. 3c). Thus, the Walker circulation is altered, with strong descending motion near 90°E (Supplementary Fig. 6b–e). This configuration allows for mild westerly wind anomalies in the western tropical Pacific from MAM$_0$, which marginally contribute to the development of modest and insignificant warm SST anomalies in the tropical Pacific (Fig. 2c–f). Nonetheless, sea level pressure near 90°W region increases from DJF$_0$ to JJA$_0$ seasons, leading to easterly wind anomalies in the eastern equatorial Pacific and cold SST anomalies along the Peru coast (Fig. 2c, d). However, given the cold mean state of the eastern tropical Pacific, local atmosphere-ocean interactions are not strong enough to further enlarge the impact of easterly wind

https://doi.org/10.1038/s41467-025-56874-y

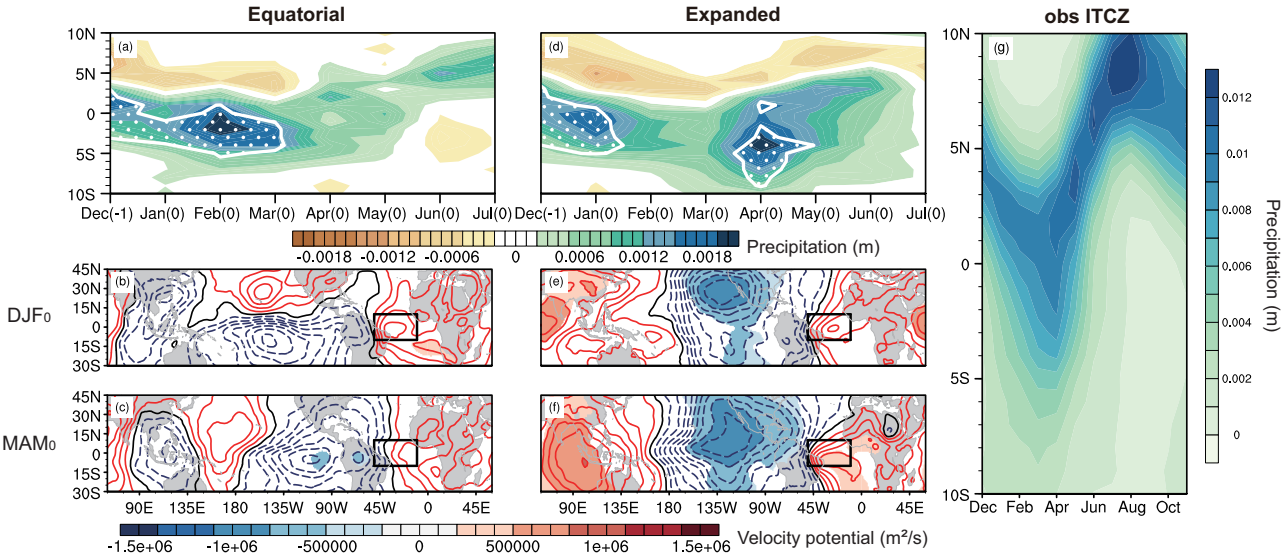

Fig. 3 | Different impacts of two types of Atlantic Niño events. Composited **a** zonal averaged precipitation anomalies (m, ERA5) over the Amazon-western tropical Atlantic region (10°S–10°N, 50°W–10°W) from December$_{-1}$ to July$_0$ and **b**, **c** 850hPa velocity potential (contour, m^2/s, interval is 10^{-7}, positive/negative values indicate convergence/divergence, ERA5) anomalies from December$_{-1}$-January$_0$-February$_0$ (DJF$_0$, where −1 and 0 represent the preceding and current year of the winter Atlantic Niño peak season) to March$_0$-April$_0$-May$_0$ (MAM$_0$) season for Equatorial Atlantic Niño events. White dotes in (**a**) and shadings in (**b**, **c**) exceed 95% significance level. The black boxes in (**b**, **c**, **e**, **f**) indicate the locations of the Amazon-western tropical Atlantic region. The influences of DJF$_0$ El Niño-Southern Oscillation (ENSO) have been removed before the composite analysis. **d**–**f** are similar to **a**–**c**, but for Expanded Atlantic Niño events. **g** Evolutions of 50°W–10°W averaged climatological precipitation (m, ERA5).

anomalies. Consequently, the cold SST anomalies are weak and confined to the coastal areas, which hardly develop into La Niña events.

In contrast, warm SST anomalies from Expanded Atlantic Niño events induce strong in-situ deep convection especially in spring, leading to low-level convergence in the Amazon-western tropical Atlantic and tropical Indian Ocean (Fig. 3e, f). The subtropical North Pacific high as well as an anticyclonic circulation get intensified in DJF$_0$ season[28,40]. On their south flank, easterly wind anomalies prevail the western tropical Pacific, further modulating the Walker circulation since MAM$_0$, with strong descending motion near the dateline and ascending motion over the Maritime Continent (Supplementary Fig. 6g–j). Easterly wind anomalies are induced in the western tropical Pacific by the SpDC mechanism, setting the stage for cold SST anomalies in the central equatorial Pacific in the following seasons (Fig. 2i–l).

Different influences of Equatorial and Expanded Atlantic Niño events in numerical model experiments

Since it might be challenging to completely eliminate the role of DJF$_0$ ENSO in observations or coupled models due to the substantial influence of ENSO, simulations from the atmospheric general circulation model (AGCM) are conducted to further validate the distinct impacts of Equatorial and Expanded Atlantic Niño events especially in regard to the SpDC mechanism (Supplementary Table 1). Initially, a CTRL_AGCM is conducted with the forcing of the fixed climatological mean SST annual cycle. The CTRL_AGCM successfully captures the seasonal meridional movement of the ITCZ (Fig. 4a), aligning well with observations (Fig. 3g) that the ITCZ reaches its southernmost latitude in spring season. Given the decent performance of the AGCM, two sensitive experiments (Equatorial_AGCM and Expanded_AGCM) are carried out to examine the different atmospheric responses to warm SST anomalies from the Equatorial and Expanded Atlantic Niño events (Supplementary Fig. 7). Figure 4b, e illustrate the differences in rainfall between the CTRL_AGCM and two sensitive experiments (the latter minus the former). During DJF$_0$ season, both the Equatorial_AGCM and Expanded_AGCM exhibit similar rainfall patterns, characterized by positive rainfall over the Amazon-western tropical Atlantic region and negative rainfall over the north equatorial Atlantic. However, from March$_0$ onwards, noticeable differences emerge between the two experiments. In the Equatorial_AGCM, positive precipitation weakens and remains confined to the equatorial region (Fig. 4b). Conversely, in the Expanded_AGCM, positive rainfall shifts to the STA region and even stronger in strength although the anomalous SST forcing weakens (Fig. 4e), confirming the SpDC mechanism that is associated with the southward migration of the ITCZ. As a result, the Expanded Atlantic Niño can induce significant easterly wind anomalies over the western-central equatorial Pacific (Fig. 4f, g), which are absent in Equatorial_AGCM (Fig. 4c, d), consistent with observations (Fig. 2b, c, h, i).

To exclude the impact of ENSO cyclic transition, we also conduct a Coupled General Circulation Model (CGCM) simulation forced by the zonal wind stress anomalies over the western-central tropical Pacific (red boxes in Fig. 4f, g) produced by the Expanded_AGCM from December$_{-1}$ to May$_0$. During the period of wind stress forcing, Niño3.4 SST in the sensitivity run is cooler than the control run since January$_0$. After the vanishment of the wind forcing since June$_0$, the La Niña condition continue to reinforce through the local air sea coupling process over the tropical Pacific. The averaged difference of Niño3.4 SST between the Expanded_CGCM and the CTRL_CGCM reaches −0.5 °C in August$_0$, further developing into −0.8 °C in the subsequent winter (Fig. 4h). The results of sensitive experiments show that the Expanded Atlantic Niño can induce La Niña, while the impact of the Equatorial Atlantic Niño is weak, which is consistent with observation.

Additionally, historical simulations from multiple state-of-the-art climate models participated in the Coupled Model Intercomparison Project Phase 6 (CMIP6, Fig. 5)[48] have been utilized to validate the distinct impacts of Equatorial and Expanded Atlantic Niño events (Supplementary Table 2). It is noteworthy that almost all models (26 out of 27) exhibited a negative correlation between the DJF$_1$ Niño3.4 index and the DJF$_0$ SST anomalies in the Equatorial Atlantic (EqA) or STA region, with 15 models having at least one regional relationship greater than 95% significance level. Consistent with the observation, two types of Atlantic Niño events are identified in CMIP6 models, and

https://doi.org/10.1038/s41467-025-56874-y

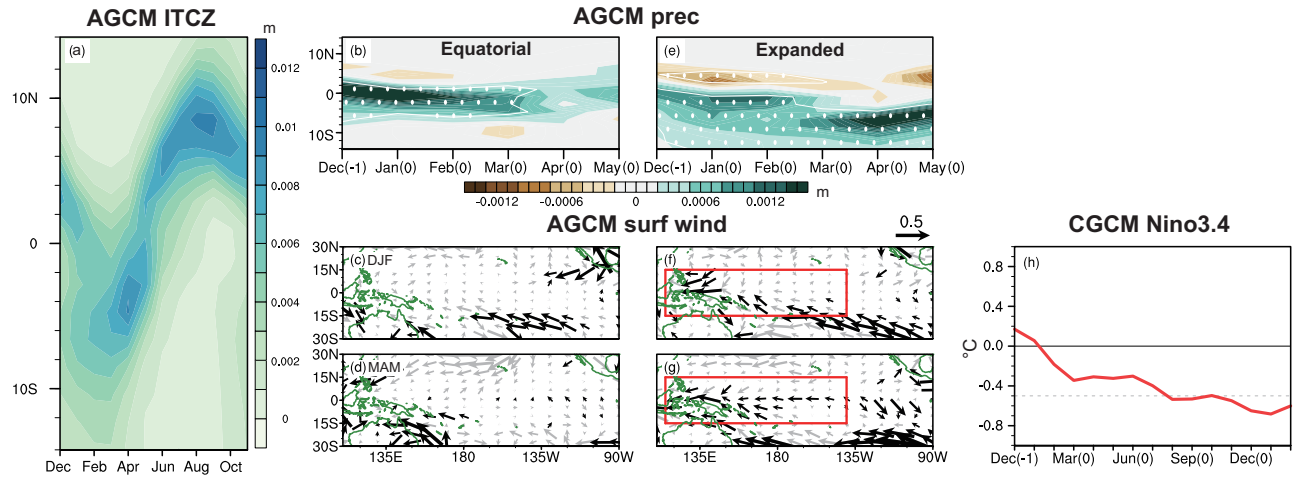

Fig. 4 | Results of sensitive experiments. a Evolutions of 50°W–10°W averaged climatological precipitation (m) from the CTRL_AGCM of Atmospheric General Circulation Model (AGCM) experiments. **b** Ensemble mean of 60°W–10°W averaged precipitation differences (m) between the Equatorial_AGCM and CTRL_AGCM. The white dots exceed 95% significance level. **c**, **d** Ensemble mean of surface wind differences (m/s) between the Equatorial_AGCM and CTRL_AGCM in December$_{-1}$-January$_0$-February$_0$ (DJF$_0$, where −1 and 0 represent the preceding and current year of the winter Atlantic Niño peak season) and March$_0$-April$_0$-May$_0$ (MAM$_0$) seasons. The black vectors exceed 95% confidence level. **e**–**g** are similar to **b**–**d**, but for the differences between the Expanded_AGCM and CTRL_AGCM. The red boxes in (**f**, **g**) indicate the range of 15°S–15°N,115°E–140°W. **h** Evolution of the Coupled General Circulation Model (CGCM) simulated sea surface temperature (°C) difference between the Expanded_CGCM and the CTRL_CGCM in Niño 3.4 region. The gray dashed line in h indicates the threshold of −0.5 °C.

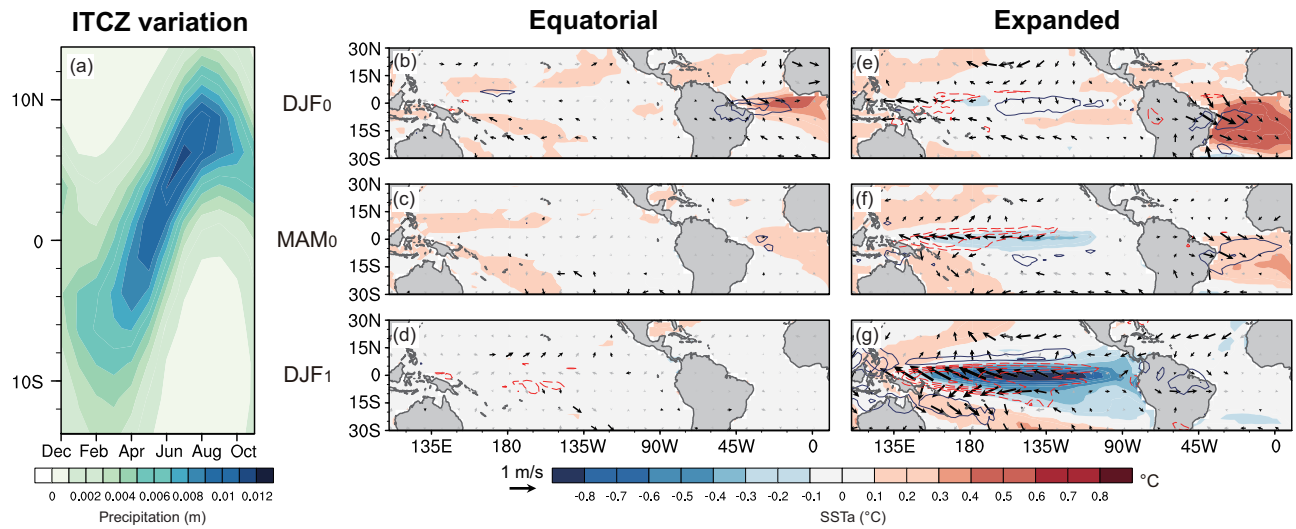

Fig. 5 | Different impacts of Equatorial and Expanded Atlantic Niño events in 27 CMIP6 historical simulations. a The ensemble mean of 50°W–10°W averaged climatological precipitation (m, CMIP6). **b**–**g** Ensemble mean of composited sea surface temperature (SST, shading, °C, only values exceed 95% significance level are given, CMIP6), surface wind (vector, m/s, black vectors exceed 95% significance level, CMIP6), and precipitation (contour, interval is 5×10^{-4} kg/m^2/s, red solid and blue dashed lines for positive and negative, CMIP6) from 27 CMIP6 historical simulations for Equatorial and Expanded types of Atlantic Niño events in December$_{-1}$-January$_0$-February$_0$ (DJF$_0$, where −1, 0, and 1 represent the preceding, current and subsequent year of the winter Atlantic Niño peak season), March$_0$-April$_0$-May$_0$ (MAM$_0$) and December$_0$-January$_1$-February$_1$ (DJF$_1$) seasons. The influences of DJF$_0$ El Niño-Southern Oscillation (ENSO) have been removed before the composite analysis.

the impacts of ENSO in DJF$_0$ season have also been removed before composite analysis.

The multi-model ensemble (MME) mean of the precipitation climatology from the 27 CMIP6 historical simulations aligns with the observed seasonal cycle of the ITCZ, although the southern edge of the rainfall center is depicted further south in the models (Fig. 5a). Most importantly, the distinct responses of the tropical Pacific to the two types of Atlantic Niño events are consistently robust across all 27 CMIP6 models. During DJF$_0$ season, warm SST anomalies are confined to the equatorial region and expand progressively from the equatorial region to 25°S for two types of events (Fig. 5b, e). The effectiveness of the two types of Atlantic Niño events in inducing atmospheric responses varies significantly, thereby affecting the following ENSO events differently. For the Equatorial events, rainfall in the Amazon-western tropical Atlantic region is weak and short-lived, only strong in DJF$_0$, causing feeble remote responses in the tropical Pacific. Weak easterly wind anomalies in the western tropical Pacific and weak cold SST anomalies in the central tropical Pacific are seen after the Equatorial Atlantic Niño (Fig. 5b–d), which are slightly different from observations (Fig. 2b–f). In contrast, for the Expanded events, the persistence of positive precipitation anomalies in the Amazon-western Atlantic is much longer than that in the Equatorial events, leading to strong easterly wind anomalies in the western tropical Pacific and cold SST anomalies in central-eastern equatorial Pacific (Fig. 5e–g). The

MME results suggest that the CMIP6 models can capture the characteristics of both types of Atlantic Niño events, although the impacts of Equatorial Atlantic Niño on the tropical Pacific are weaker.

It should be noted that models (include AGCM and CMIP6) show inadequate simulations of the seasonal shifts of the ITCZ in timing and location (Figs. 4a and 5a), which may result in errors in models wind stress and air-sea coupling strength[49,50]. The latitudinal positions of the climatological ITCZ and model simulated regression of precipitation anomalies on the underlying SST anomalies over the STA region are compared to display the precipitation sensitivity to anomalous surface heating (Supplementary Fig. 8). Since the SST is fixed annually in the self-conducted AGCM experiments, outputs from the CMIP5-CAM5 Atmospheric Model Intercomparison Project (AMIP) experiment[51] are adopted for the comparison of precipitation sensitivity.

Compared with observations, there is a noticeable bias in models, particularly among the coupled models. The CMIP6 models exhibit substantial discrepancies during the DJF season, extending further south (approximately 6–7°). The CGCM_CTRL experiment demonstrates a southward bias of around 3° from December through June. Relatively, atmospheric models (AMIP outputs and AGCM_CTRL), which are forced by observed SST, display a more realistic seasonal cycle of the Atlantic ITCZ latitude, with northward bias about 1° in the MAM season. However, although the ITCZ being positioned further south in the coupled models, the precipitation response to SST anomalies in the STA region is not more pronounced than in observations (Supplementary Fig. 8b–i, k, l), suggesting that the southward bias of ITCZ locations in models would not exaggerate the role of SpDC mechanism in the model simulations. However, although the ITCZ being positioned further south in the coupled models, the local precipitation and Pacific wind responses to the STA SST anomalies are not more pronounced than in observations (Supplementary Fig. 9), suggesting that the southward bias of ITCZ locations in model simulations would not exaggerate the role of SpDC mechanism on causing atmospheric responses in the Pacific.

Discussion

In the present study, we revisit the relationship between winter Atlantic Niño/Niña and subsequent ENSO occurrences and identify potential key factors within the SST anomalies in the STA region that may play a crucial role in determining the impacts of winter Atlantic Niño on ensuing La Niña events. Our analysis reveals that the presence of SST anomalies in the STA region acts as a determining factor in differentiating between two distinct groups of winter Atlantic Niño events: the Equatorial type and the Expanded type. Notably, these two types of Atlantic Niño events cause contrasting responses in the tropical Pacific region, primarily due to their varying abilities to induce diabatic heating anomalies in situ during the following spring season. Associated with the seasonal modulation of the tropical Atlantic mean state, the southward shift of the ITCZ during the boreal spring season creates a conducive environment for the Expanded Atlantic Niño SST anomalies to generate diabatic heating and influence atmospheric circulation, a phenomenon referred to as the Spring Deep Convection (SpDC) mechanism in our study. This mechanism has been further substantiated through a series of AGCM and CGCM experiments. By significantly impacting the Walker circulation and triggering zonal wind anomalies in the western tropical Pacific region, the Expanded Atlantic Niño events can induce La Niña-like SST cooling patterns in the subsequent seasons, thereby illustrating the complex interplay between Atlantic and Pacific climate phenomena.

What differentiates the Equatorial from Expanded Atlantic Niño events is the warming in the STA region. The role of STA is further investigated by examining the characteristics of "pure" STA events in the absence of equatorial SST warming (Supplementary Fig. 10). Specifically, a total of 8 STA events were identified from 1950 to 2022, with 6 of them following cold SST anomalies in Niño 3.4 region in the subsequent winter season (Supplementary Fig. 10a). However, the strength of cold Niño 3.4 SST anomaly is much weaker than its counterpart from the Expanded Atlantic Niño (Fig. 2g). The responses of precipitation to warm SST anomalies in the STA are relatively weak in DJF_0 but significantly intensifies in MAM_0 when the ITCZ shifts southward (Supplementary Fig. 11a). The velocity potential and surface wind anomalies induced in the tropical Pacific by the STA warm SST anomalies are characterized as a similar pattern to Expanded type Atlantic Niño events, albeit with reduced intensity (Supplementary Figs. 10b–d and 11b, c). As a result, the STA events lead to milder SST cooling in the tropical Pacific compared to the Expanded type events (Fig. 2h–l). The "pure" STA events from CMIP6 historical simulations exhibit consistency with observations (Supplementary Fig. 12), characterized by a similar pattern to Expanded type Atlantic Niño events but with reduced intensity.

To enhance our understanding, we have also categorized Atlantic Niña events into two distinct types. The analysis reveals a significant distinction between the Equatorial/Expanded Atlantic Niña events and their positive counterparts in terms of their influence over the tropical Pacific, with both types of Atlantic Niña are followed by El Niño events (Supplementary Fig. 13). Specifically, the cold SST anomalies associated with the Equatorial Atlantic Niña events are accompanied by cooling in the north tropical Atlantic (NTA) region from DJF_0 to JJA_0 (Supplementary Fig. 13a–c). With the presence of NTA cooling, the Equatorial Atlantic Niña could potentially trigger El Niño through exerting Rossby wave[21,52]. In contrast, the Expanded Atlantic Niña display cold SST anomalies that mirror the conditions of their positive phase throughout their duration, which also fosters an El Niño-like response in the Pacific. The composite results of both Equatorial and Expanded Atlantic Niña events reaffirm previous research indicating that the NTA has a more robust connection with the subsequent ENSO compared with the equatorial region[20].

In addition, previous studies have pointed out that the South Atlantic Subtropical Dipole (SASD) which manifests as warm SST anomalies in the northeast pole (30°S–20°S, 40°W–20°E) and opposite SST anomalies in the southwest pole (45°S–35°S, 60°W–0°)[53–55], could exert significant influences on the Atlantic Niño events[56,57] and subsequent ENSO[58]. Although both the SASD and the Expanded Atlantic Niño we proposed have incorporated the subtropical SST anomalies into the mechanism through which the Atlantic impacts the Pacific, discrepancies exist in their areas of focus. The SASD underlines that the extratropical SST anomalies can induce the SST anomalies in the equatorial Atlantic with the seasonal evolution, which subsequently influence the Pacific ENSO. By contrast, the Expanded Atlantic Niño emphasizes that in spring, the STA SST anomalies, along with the southward shift of climatological precipitation, can effectively activate the convective response in conjunction with the equatorial SST anomalies, thereby more robustly promoting the influence of the Atlantic Ocean on ENSO.

Although both the SASD and the Expanded Atlantic Niño on subsequent La Niña events is similar to that of negative SASD as both influence ENSO through changes in local convective activities and modulation of Walker circulation. However, the relationship between equatorial Atlantic SST anomalies and ENSO is unstable and conditional. During MAM season, accompanied by seasonal southward movement of ITCZ, the Expanded Atlantic Niño can persistently induce strong positive precipitation, leading to adjustments in Walker Cell dynamics and ultimately favoring La Niña development. In contrast, without warming in the subtropical South Atlantic region, the Equatorial Atlantic Niño has much weaker impacts in modulating Walker circulation and subsequent La Niña events. In essence, the interaction between the mean climate state and anomalous fields plays a dual role in shaping the effects of STA SST anomalies. While the southward displacement of the ITCZ in $sping_0$ facilitates the SpDC response to

STA warming, its northern location in DJF_0 reduces the capacity of stronger STA warming in this season to induce diabatic heating anomalies. Consequently, although the Equatorial Atlantic Niño events have limited influence on subsequent La Niña occurrences, the presence of warm SST anomalies in the equatorial region is deemed significant for the pronounced impacts of Expanded Atlantic Niño events on the Pacific, or even global climate dynamics.

Lastly, it is worth emphasizing that the inherent characteristics of ENSO will unavoidably play a role in triggering the subsequent La Niña events. Consequently, although the Expanded Atlantic Niño might have an impact on modulating the atmospheric circulation over the Pacific, it remains challenging to precisely evaluate the comparative significance of the Expanded Atlantic Niño and the self-oscillation of ENSO in giving rise to the subsequent La Niña. These complex interactions between the Atlantic and Pacific will constitute the principal emphasis of our forthcoming research endeavors, yet beyond the purview of the current study.

Methods

Observations and model data sets

The SST dataset from 1950 to 2022 is derived from Expanded Reconstructed Sea Surface Temperature version 5 (ERSSTv5) with a 2.5° spatial resolution[59]. The atmospheric variables (wind and rainfall) used in this study are from the European Centre for Medium-range Weather Forecast (ECMWF) reanalysis (ERA5)[60], which spans from 1950 to 2022 on a 1° spatial resolution. The 20 °C isotherm depth is calculated from IAP global ocean temperature gridded product, with 1° × 1° horizontal resolution and 41 vertical levels from 1 to 2000 m[61].

To confirm the roles of Equatorial and Expanded Atlantic Niño and enlarge the sample size, 27 CMIP6 coupled global climate models (Table. S2) under historical radiative forcing are analyzed. CMIP6 outputs cover 65 years from 1950 to 2014. Based on the relationship between the DJF_0 Atlantic Niño/Niña and DJF_1 ENSO, 15 models that can capture the significant negative connection between the tropical Atlantic SST anomalies and the next ENSO are selected finally. The horizontal resolutions of the 15 models are interpolated into 2.5° (longitude) × 2.5° (latitude).

The CESM2 Pacific Pacemaker experiment comprises a 10-member ensemble of CESM2 simulations, designed to align the model's SST anomalies with observed data in the central-eastern tropical Pacific region. In the East Pacific, nudging is applied with full intensity between 15°S and 15°N, stretching from the dateline to the American coast, with a 5° latitude buffer zone to the south and north where the strength of the relaxation decreases linearly. Beyond the dateline, the nudging mask takes on a wedge shape, tapering off in latitude as it approaches the Maritime Continue. This allows the rest of the model's coupled climate system to evolve autonomously, simulating a more realistic interaction with the observed ENSO dynamics. All CMIP6 time-varying external, natural and anthropogenic forcings were specified in this ensemble, using historical forcings in 1880–2014 simulations, and SSP3-7.0 forcing in 2015–2019 simulations.

The EqA region locates in 20°W–0°, 5°S–5°N, slightly wider than ATL3 region (20°W–0°, 3°S–3°N). The STA region is 60°W–10°E, 20°S–5°S. The Equatorial Atlantic Niño is defined as a positive SST anomaly in the EqA region that exceeds its 0.75 std but does not exceed this threshold in the STA region. The Expanded Atlantic Niño is identified as warm SST anomalies in both the EqA and STA regions exceeding their 0.75 std. The pure STA event is defined as only warm SST anomaly in the STA region that exceeds its 0.75 std, without exceeding this threshold in the EqA region. The strength of ENSO is represented by SST anomalies over the Niño3.4 region (120°W–170°W and 5°S–5°N) in DJF_1. The signals of DJF_0 ENSO have been removed in the composite analysis by linear partial regression on DJF_0 Niño3.4 SST anomalies. All anomalies are detrended to remove the influence of global warming.

The Atlantic ITCZ latitude is calculated in the region of 60°W–10°W 15°S–15°N as a precipitation-weighted mean[49,50], as follows:

$$\varnothing_{ITCZ} = \sum_i \frac{Precip_{60\,^\circ W-10\,^\circ W} \cdot \varnothing_i}{Precip_{60\,^\circ W-10\,^\circ W,\,15\,^\circ S-15\,^\circ N}} \quad (1)$$

where $Precip_{60\,^\circ W-10\,^\circ W}$ is the zonally summed precipitation at latitude $\varnothing_i$, $Precip_{60\,^\circ W-10\,^\circ W,\,15\,^\circ S-15\,^\circ N}$ is the sum of precipitation of whole 60°W–10°W 15°S–15°N region.

In this study, the Student's *t*-test is conducted for composite analyses. For CMIP6 models, the 95% confidence level of MME anomalies is calculated as follows[62]:

$$|Var_{MME}| \geq \frac{std \times \lambda}{\sqrt{n}} \quad (2)$$

Where $|Var_{MME}|$ and *std* are absolute value and intermodal standard deviation of the MME variable anomalies. *n* is the number of models and λ is 1.96.

Model experiments

AGCM experiments. To investigate the different impacts of Equatorial and Expanded Atlantic Niño events, three AGCM experiments are performed by using CAM4 of CESM[46]: one is a control (AGCM_CTRL) and the other two are sensitivity experiments (Equatorial and Expanded). The AGCM_CTRL is forced by global monthly climatological SST implemented with F2000 component sets. Sensitivity experiments are identical to AGCM_CTRL except that the observed warm SST anomalies are prescribed in the only EqA region, both EqA and STA region from $December_{-1}$ to May_0. The AGCM experiments have a horizontal resolution of 1.9° × 2.5°and include 26 vertical levels. All AGCM experiments are integrated for 50 years, and the ensemble mean of the last 20 years is used in the present study.

CGCM experiments. The CGCM used in the present study is from CESM 1.2.2[63]. The atmospheric component is CAM4 and the ocean model is the Parallel Ocean Program (POP) with a horizontal resolution of 0.5° latitude × 0.9° longitude and 60 vertical levels. In order to reveal the impacts of the wintertime and springtime forcing of the Equatorial Atlantic Niño on the Pacific and to remove the influences of previous ENSO, two sets of idealized CGCM experiments are designed. The first one is a control simulation (CTRL_CGCM), which is integrated for 1100 years to eliminate climate shifts. The 999–1100 period is used in the present study. The second one is a sensitivity experiment (Expanded_CGCM). The zonal wind during $December_{-1}$-May_0 forced by Expanded type Atlantic Niño from AGCM results is added onto the climatological mean zonal wind over the central-western tropical Pacific (Fig. 4f, g), while the remaining region is prescribed with climatological zonal wind. The added zonal wind pattern is based on monthly data and linearly interpolated into daily data. The sensitivity experiment run is from 1st $December_{-1}$ to 31st $February_1$ for each member and it includes 50 members. The initial condition for the first member is chosen as December in the year 999, the next in the year 1001, and so on.

Data availability

Data relevant to this study can be downloaded from the following websites: ERSST v5: https://psl.noaa.gov/data/gridded/index.html. ERA5: https://www.ecmwf.int/en/forecasts/dataset/ecmwf-reanalysis-v5; CMIP6 database at https://esgf-node.llnl.gov/projects/cmip6/. IAP: http://www.ocean.iap.ac.cn/pages/dataService/dataService.html. CESM2 Pacific Pacemaker Ensemble outputs: https://www.cesm.ucar.edu/working-groups/climate/simulations/cesm2-pacific-pacemaker. The scripts used to analyze data and the numerical model results in this

study are available from the corresponding author upon request. The experiments data generated in this study have been deposited in the Code Ocean website https://doi.org/10.24433/co.9447850.v1.

Code availability

Codes used in the manuscript are available on the Code Ocean website https://doi.org/10.24433/co.9447850.v1.

References

1. Philander, S. G. H. Unusual conditions in the tropical Atlantic Ocean in 1984. *Nature* **322**, 236–238 (1986).
2. Zebiak, S. E. Air–Sea interaction in the Equatorial Atlantic Region. *J. Clim.* **6**, 1567–1586 (1993).
3. Chang, P., Fang, Y., Saravanan, R., Ji, L. & Seidel, H. The cause of the fragile relationship between the Pacific El Nĩo and the Atlantic Nĩo. *Nature* **443**, 324–328 (2006).
4. Lübbecke, J. F. Climate science: tropical Atlantic warm events. *Nat. Geosci.* **6**, 22–23 (2013).
5. Tan, W., Liu, Y., Li, X., Johnson, N. C. & Hu, Z. Z. Multi-time scale variations in atlantic niño and a relative atlantic niño index. *Geophys. Res. Lett.* **50**, e2023GL106511 (2023).
6. Koseki, S., Tjiputra, J., Fransner, F., Crespo, L. R. & Keenlyside, N. S. Disentangling the impact of Atlantic Niño on sea-air CO2 flux. *Nat. Commun.* **14**, 1–8 (2023).
7. Lübbecke, J. F. & McPhaden, M. J. Symmetry of the Atlantic Niño mode. *Geophys. Res. Lett.* **44**, 965–973 (2017).
8. Okumura, Y. & Xie, S. P. Some overlooked features of tropical atlantic climate leading to a new Niño-like phenomenon. *J. Clim.* **19**, 5859–5874 (2006).
9. Hounsou-Gbo, A., Servain, J., Vasconcelos Junior, FdasC., Martins, E. S. P. R. & Araújo, M. Summer and winter Atlantic Niño: connections with ENSO and implications. *Clim. Dyn.* **55**, 2939–2956 (2020).
10. Vallès-Casanova, I., Lee, S. K., Foltz, G. R. & Pelegrí, J. L. On the spatiotemporal diversity of Atlantic Niño and associated rainfall variability over West Africa and South America. *Geophys. Res. Lett.* **47**, 1–10 (2020).
11. Kim, D. et al. Increase in Cape Verde hurricanes during Atlantic Niño. *Nat. Commun.* **14**, 3704 (2023).
12. Losada, T. et al. A multi-model approach to the Atlantic Equatorial mode: Impact on the West African monsoon. *Clim. Dyn.* **35**, 29–43 (2010).
13. Giannini, A., Saravanan, R. & Chang, P. Oceanic forcing of sahel rainfall on interannual to interdecadal time scales. *Science* **302**, 1027–1030 (2003).
14. Chen, B., Zhang, L. & Wang, C. Distinct impacts of the Central and Eastern Atlantic Niño on the European Climate. *Geophys. Res. Lett.* **51**, e2023GL107012 (2024).
15. Kucharski, F., Bracco, A., Yoo, J. H. & Molteni, F. Atlantic forced component of the Indian monsoon interannual variability. *Geophys. Res. Lett.* **35**, L04706 (2008).
16. Kucharski, F. et al. A Gill-Matsuno-type mechanism explains the tropical Atlantic influence on African and Indian monsoon rainfall. *Q. J. R. Meteorol. Soc.* **135**, 569–579 (2009).
17. Wang, C., Kucharski, F., Barimalala, R. & Bracco, A. Teleconnections of the tropical Atlantic to the tropical Indian and Pacific Oceans: a review of recent findings. *Meteorol. Z.* **18**, 445–454 (2009).
18. Lübbecke, J. F. et al. Equatorial Atlantic variability—Modes, mechanisms, and global teleconnections. *Wiley Interdiscip. Rev. Clim. Chang.* **9**, 2017–2018 (2018).
19. Yadav, R. K., Srinivas, G. & Chowdary, J. S. Atlantic Niño modulation of the Indian summer monsoon through Asian jet. *npj Clim. Atmos. Sci.* **1**, 23 (2018).
20. Ham, Y. G., Kug, J. S. & Park, J. Y. Two distinct roles of Atlantic SSTs in ENSO variability: North Tropical Atlantic SST and Atlantic Niño. *Geophys. Res. Lett.* **40**, 4012–4017 (2013).
21. Jiang, L. & Li, T. Impacts of tropical North Atlantic and Equatorial Atlantic SST anomalies on ENSO. *J. Clim.* **34**, 5635–5655 (2021).
22. Keenlyside, N. S., Ding, H. & Latif, M. Potential of equatorial Atlantic variability to enhance El Niño prediction. *Geophys. Res. Lett.* **40**, 2278–2283 (2013).
23. Kucharski, F., Syed, F. S., Burhan, A., Farah, I. & Gohar, A. Tropical Atlantic influence on Pacific variability and mean state in the twentieth century in observations and CMIP5. *Clim. Dyn.* **44**, 881–896 (2015).
24. Chikamoto, Y., Johnson, Z. F., Wang, S. Y. S., McPhaden, M. J. & Mochizuki, T. El Niño–Southern oscillation evolution modulated by Atlantic forcing. *J. Geophys. Res. Ocean.* **125**, 1–15 (2020).
25. Frauen, C. & Dommenget, D. Influences of the tropical Indian and Atlantic Oceans on the predictability of ENSO. *Geophys. Res. Lett.* **39**, 2–7 (2012).
26. Exarchou, E. et al. Impact of equatorial Atlantic variability on ENSO predictive skill. *Nat. Commun.* **12**, 1612 (2021).
27. Fan, H., Wang, C., Yang, S. & Zhang, G. Coupling is key for the tropical Indian and Atlantic oceans to boost super El Niño. *Sci. Adv.* **10**, 1–8 (2024).
28. Park, J. H. et al. Distinct decadal modulation of Atlantic-Niño influence on ENSO. *npj Clim. Atmos. Sci.* **6**, 105 (2023).
29. Polo, I., Martin-Rey, M., Rodriguez-Fonseca, B., Kucharski, F. & Mechoso, C. R. Processes in the Pacific La Niña onset triggered by the Atlantic Niño. *Clim. Dyn.* **44**, 115–131 (2015).
30. Zhang, L. et al. Emergence of the Central Atlantic Niño. *Sci. Adv.* **9**, 1–10 (2023).
31. Rodríguez-Fonseca, B. et al. Are Atlantic Niños enhancing Pacific ENSO events in recent decades? *Geophys. Res. Lett.* **36**, 1–6 (2009).
32. Wang, C. Three-ocean interactions and climate variability: a review and perspective. *Clim. Dyn.* **53**, 5119–5136 (2019).
33. Cai, W. et al. Pantropical climate interactions. *Science* **363**, eaav4236 (2019).
34. Liu, S., Chang, P., Wan, X., Yeager, S. G. & Richter, I. Role of the Maritime Continent in the remote influence of Atlantic Niño on the Pacific. *Nat. Commun.* **14**, 3327 (2023).
35. Richter, I., Tokinaga, H., Kosaka, Y., Doi, T. & Kataoka, T. Revisiting the Tropical Atlantic Influence on El Niño–Southern Oscillation. *J. Clim.* **34**, 8533–8548 (2021).
36. Ding, H., Keenlyside, N. S. & Latif, M. Impact of the Equatorial Atlantic on the El Niño Southern Oscillation. *Clim. Dyn.* **38**, 1965–1972 (2012).
37. Losada, T. & Rodríguez-Fonseca, B. Tropical atmospheric response to decadal changes in the Atlantic Equatorial Mode. *Clim. Dyn.* **47**, 1211–1224 (2016).
38. Wang, R., He, J., Luo, J. J. & Chen, L. Atlantic warming enhances the influence of Atlantic Niño on ENSO. *Geophys. Res. Lett.* **51**, e2023GL108013 (2024).
39. Martín-Rey, M., Rodríguez-Fonseca, B., Polo, I. & Kucharski, F. On the Atlantic–Pacific Niños connection: a multidecadal modulated mode. *Clim. Dyn.* **43**, 3163–3178 (2014).
40. Park, J. H. et al. Significant winter Atlantic Niño effect on ENSO and its future projection. *npj Clim. Atmos. Sci.* **7**, 1–8 (2024).
41. Seager, R. et al. Air-sea interaction and the seasonal cycle of the subtropical anticyclones. *J. Clim.* **16**, 1948–1966 (2003).
42. Cabos, W. et al. The South Atlantic Anticyclone as a key player for the representation of the tropical Atlantic climate in coupled climate models. *Clim. Dyn.* **48**, 4051–4069 (2017).
43. Lübbecke, J. F., Böning, C. W., Keenlyside, N. S. & Xie, S. P. On the connection between Benguela and equatorial Atlantic Nios and the role of the South Atlantic Anticyclone. *J. Geophys. Res. Ocean.* **115**, 1–16 (2010).
44. Sun, X., Vizy, E. K. & Cook, K. H. Land–atmosphere–ocean interactions in the southeastern Atlantic: interannual variability. *Clim. Dyn.* **52**, 539–561 (2019).

45. Florenchie, P., Lutjeharms, J. R. E., Reason, C. J. C., Masson, S. & Rouault, M. The source of Benguela Niños in the South Atlantic Ocean. *Geophys. Res. Lett.* **30**, 10–13 (2003).
46. Li, X., Tan, W., Hu, Z. Z. & Johnson, N. C. Evolution and prediction of two extremely strong Atlantic Niños in 2019–2021: Impact of Benguela warming. *Geophys. Res. Lett.* **50**, e2023GL104215 (2023).
47. Jiang, F. et al. Resolving the Tropical Pacific/Atlantic interaction Conundrum. *Geophys. Res. Lett.* **50**, e2023GL103777 (2023).
48. Ferraro, R., Waliser, D. E., Gleckler, P., Taylor, K. E. & Eyring, V. Evolving Obs4MIPs to support phase 6 of the coupled model inter comparison project (CMIP6). *Bull. Am. Meteorol. Soc.* **96**, 131–133 (2015).
49. Good, P., Boers, N., Boulton, C. A., Lowe, J. A. & Richter, I. How might a collapse in the Atlantic Meridional Overturning Circulation affect rainfall over tropical South America? *Clim. Resil. Sustain.* **1**, 1–13 (2022).
50. Ben-Yami, M. et al. Impacts of AMOC collapse on Monsoon rainfall: a multi-model comparison. *Earth's Futur.* **12**, e2023EF003959 (2024).
51. Taylor, K. E., Stouffer, R. J. & Meehl, G. A. An overview of CMIP5 and the experiment design. *Bull. Am. Meteorol. Soc.* **93**, 485–498 (2012).
52. Ham, Y. G., Kug, J. S., Park, J. Y. & Jin, F. F. Sea surface temperature in the north tropical Atlantic as a trigger for El Niño/Southern Oscillation events. *Nat. Geosci.* **6**, 112–116 (2013).
53. Morioka, Y., Tozuka, T. & Yamagata, T. On the Growth and Decay of the Subtropical Dipole Mode in the South Atlantic. *J. Clim.* **24**, 5538–5554 (2011).
54. Venegas, S. A., Mysak, L. A. & Straub, D. N. Atmosphere-ocean coupled variability in the South Atlantic. *J. Clim.* **10**, 2904–2920 (1997).
55. Venegas, S. A., Mysak, L. A. & Straub, D. N. Evidence for interannual and interdecadal climate variability in the South Atlantic. *Geophys. Res. Lett.* **23**, 2673–2676 (1996).
56. Grimm, A. M. & Reason, C. J. C. Does the South American monsoon influence African rainfall? *J. Clim.* **24**, 1226–1238 (2011).
57. Nnamchi, H. C. et al. An equatorial-extratropical dipole structure of the Atlantic Niño. *J. Clim.* **29**, 7295–7311 (2016).
58. Ham, Y. G. et al. Inter-basin interaction between variability in the South Atlantic Ocean and the El Niño/Southern oscillation. *Geophys. Res. Lett.* **48**, 1–11 (2021).
59. Huang, B. et al. Extended reconstructed Sea surface temperature, Version 5 (ERSSTv5): upgrades, validations, and intercomparisons. *J. Clim.* **30**, 8179–8205 (2017).
60. Hersbach, H. et al. The ERA5 global reanalysis. *Q. J. R. Meteorol. Soc.* **146**, 1999–2049 (2020).
61. Cheng, L. et al. Improved estimates of ocean heat content from 1960 to 2015. *Sci. Adv.* **3**, e1601545 (2017).
62. Fan, H., Yang, S., Wang, C., Wu, Y. & Zhang, G. Strengthening amplitude and impact of the pacific meridional mode on ENSO in the warming climate depicted by CMIP6 models. *J. Clim.* **35**, 5195–5213 (2022).
63. Hurrell, J. W. et al. The community earth system model: a framework for collaborative research. *Bull. Am. Meteorol. Soc.* **94**, 1339–1360 (2013).

Acknowledgements

We thank Dr. Qihua Peng and Dr. Gayan Pathirana for their help in improving our results. This research was supported by National Natural Science Foundation of China (Grant Nos. 41925024 and 92158204), National Key Research and Development Program of China (2023YFF0805300). G.Z. is supported by the National Natural Science Foundation of China (No. 42306012) and China Postdoctoral Science Foundation (2024T171069). J.C. is supported by the National Key Research and Development Program of China (2020YFA0608803), National Natural Science Foundation of China (42276031), Science and Technology Projects in Guangzhou (2024A04J9141) and Youth Innovation Promotion Association CAS. H.F. is supported by the National Natural Science Foundation of China (42206026). M.C. is supported by the Natural Science Foundation of Guangdong Province (2023A1515012145), the Science and Technology Program of Guangzhou China (2024A04J3880). X.W., L.Z., and H.F. are supported by the National Natural Science Foundation of China (W2441014), Special Fund of South China Sea Institute of Oceanology of the Chinese Academy of Sciences (SCSIO2023QY01), and Development Fund of South China Sea Institute of Oceanology of the Chinese Academy of Sciences. L.Z. is supported by the GuangDong Basic and Applied Basic Research Foundation (2024B1515040024) and the Development fund (SCSIO202203) of South China Sea Institute of Oceanology of the Chinese Academy of Sciences.

Author contributions

D.W. and X.W. conceived the idea. G.Z. and J.C. conducted the analysis and wrote the majority of the manuscript. H.F. performed the experiments. M.C. and L.Z. improved the manuscript. G.Z. and J.C. are co-first authors.

Competing interests

The authors declare no competing interests.

Additional information

Supplementary information The online version contains supplementary material available at https://doi.org/10.1038/s41467-025-56874-y.

Correspondence and requests for materials should be addressed to Xin Wang or Dongxiao Wang.

Peer review information *Nature Communications* thanks the anonymous reviewers for their contribution to the peer review of this work. A peer review file is available.